Journal of Catalysis 271 (2010) 140–152

Contents lists available at ScienceDirect

Journal of Catalysis

journal homepage: www.elsevier.com/locate/jcat

Influence of thiophene on the isooctane reforming activity of Ni-based catalysts

Joseph M. Mayne, Andrew R. Tadd, Kevin A. Dahlberg, Johannes W. Schwank *

Transportation Energy Center, Department of Chemical Engineering, University of Michigan, Ann Arbor, MI 48109, USA

ARTICLE INFO

Article history:
Received 28 August 2009
Revised 19 November 2009
Accepted 11 February 2010
Available online 16 March 2010

Keywords:
Nickel
Ceria–Zirconia
Sulfur poisoning
Autothermal reforming
Partial oxidation
Steam reforming
Isooctane

ABSTRACT

Catalytic reforming of liquid hydrocarbon fuels is challenging due to potential deactivation via carbon deposition and sulfur poisoning. To gain a better understanding of the effect of sulfur on the deactivation of $Ni/Ce_{0.75}Zr_{0.25}O_2$ catalysts, isooctane conversion to syngas was studied in the presence of small amounts of thiophene under various O/C and H_2O/C ratios representing steam reforming, partial oxidation, and autothermal reforming conditions. It was found that depending on the reaction conditions, thiophene underwent different degrees of desulfurization, leading to the formation of H_2S. Under reaction conditions leading to nearly complete conversion of thiophene to H_2S, the nickel catalyst lost only a small amount of its initial activity, but then maintained stable performance over longer times on stream. In contrast, reaction conditions under which thiophene emerged unconverted from the reactor led to severe and continued deactivation of the catalysts. Furthermore, co-feeding thiophene with isooctane caused significant increases in the temperature profile of the reactor and an increased amount of olefins were seen as products of the reaction, indicating that sulfur deactivated primarily catalyst sites responsible for endothermic steam reforming reactions, while having less impact on exothermic partial oxidation reactions. Controlling the reaction conditions in such a way as to generate sufficient hydrogen concentrations in the catalyst bed for effectively desulfurizing thiophene to H_2S appears to be the key to maintain stable catalytic activities in the presence of sulfur compounds.

1. Introduction

Several energy-related technologies such as auxiliary power units, cold-start engine ignition, and emission control could benefit from the processing of liquid fuels, such as gasoline, into hydrogen-rich streams. Possible catalytic reforming approaches include steam reforming (1), partial oxidation (2), and autothermal reforming (3). Steam reforming (SR) is the common large-scale production route for synthesis gas from methane and produces the most hydrogen of the three reforming options by reacting hydrocarbon fuels with an excess of steam. Partial oxidation (POX) employs a sub-stoichiometric co-feed of oxygen and results in a lower yield of hydrogen than SR. The autothermal reforming (ATR) reaction offers a compromise between the prohibitive heat transfer demands of steam reforming and the excessive carbon deactivation of partial oxidation, with the added benefit of a tunable process heat duty [1].

$$C_xH_y + xH_2O \rightarrow \left(\frac{y}{2} + x\right)H_2 + xCO \quad (1)$$

$$C_xH_y + \frac{x}{2}O_2 \rightarrow \frac{y}{2}H_2 + xCO \quad (2)$$

$$C_xH_y + (x-2z)H_2O + zO_2 \rightarrow \left(\frac{y}{2} + x - 2z\right)H_2 + xCO \quad (3)$$

Autothermal reforming of various hydrocarbons has previously been investigated on both noble and non-noble metal-based catalysts [2–8]. While noble metal catalysts generally offer higher activity and lower carbon formation than non-noble metals, their implementation may be cost-prohibitive. The use of nickel in reforming catalysis is attractive from an economic perspective, but Ni catalysts have several significant drawbacks that limit their performance [9], including carbon deposition, loss of active sites due to nickel particle growth or sintering, and sulfur poisoning. Carbon deposition on Ni-based catalysts can be inhibited by supporting the metal on a zirconia-modified ceria support, whose redox behavior helps decrease the amount of carbon formed during reforming reactions [10–12].

Perhaps the most intractable impediment to catalytic fuel reforming is the challenge posed by sulfur poisoning. Mercaptans, thiophenes, benzothiophenes, and dibenzothiophenes are found as contaminants or additives at various concentrations in the major hydrocarbon-based feeds to proposed fuel-reforming systems. The interaction of these species with the catalyst can lead to active-site poisoning. Such behavior has been shown to be long-range in character; consequently, even low levels of sulfur exposure (less than 1 ppmv) can cause significant changes in catalyst activity and selectivity [13]. The development of more sulfur-tolerant reformers hinges on the ability to understand the interaction of these sulfur contaminants on a complex chemical system.

* Corresponding author. Fax: +1 734 763 0459.
E-mail address: schwank@umich.edu (J.W. Schwank).

0021-9517/$ - see front matter © 2010 Elsevier Inc. All rights reserved.
doi:10.1016/j.jcat.2010.02.018

The goal of the current research is to develop a better understanding of the effect of sulfur on Ni-based ATR catalysts. The effectiveness of Ni supported on $Ce_{0.75}Zr_{0.25}O_2$ (CZO) for the ATR of 2,2,4-trimethylpentane and *n*-dodecane under sulfur-free conditions has been reported previously [14,15]. In the current study, the influence of thiophene on the reforming of isooctane is investigated under a range of ATR conditions, and under pure POX and SR conditions. Substantial progress was made toward the understanding of sulfur deactivation in catalytic fuel reformers through novel analytical and experimental strategies. Reaction conditions were chosen, which bounded typical reforming experiments and considered stoichiometric and thermodynamic equilibrium limitations. The *in situ* temperature profiles of the reformer, the identification and quantification of sulfur-containing products leaving the reactor, and the analysis of catalyst morphology provided a more thorough description of reforming behavior in the presence of sulfur.

2. Experimental

2.1. Catalyst preparation

For the purposes of this study, a single batch of 10 wt.% Ni supported on CZO was prepared. This loading level is higher than has been previously recommended for optimal carbon deposition behavior [15] but was deliberately selected for this study because the larger Ni crystals that result are easily characterized with X-ray diffraction (XRD) and scanning electron microscopy (SEM). The support was prepared by the co-precipitation of Ce and Zr from $Ce(NO_3)_3{\cdot}6H_2O$ and $ZrOCl_2{\cdot}8H_2O$ in de-ionized (DI) water, using a 4 M solution of NH_4OH as a precipitating agent. The precipitate was filtered and washed with DI water and then calcined in air at a temperature of 900 °C for 2 h. The support material was impregnated with an aqueous solution of $Ni(NO_3)_2{\cdot}6H_2O$ via incipient wetness. The catalyst precursor was then calcined at 900 °C for 2 h. The calcination temperature was chosen such that it exceeded maximum catalyst bed temperatures during reforming experiments and was intended to thermally stabilize the material. The Ni/CZO catalyst was size-fractioned, and particles between 250 and 420 microns were retained for study. Particles of this size were found to give the most favorable flow behavior during reforming experiments, preventing catalyst-bypass and excessive pressure drop in the reactor.

2.2. Reforming experiments

2.2.1. Experimental design

The prepared catalyst was tested for activity to reforming of isooctane, a surrogate for gasoline, under sulfur-free conditions and with thiophene present. Table 1 shows the experimental reforming conditions considered. In each experiment, 500 mg of catalyst was loaded into the reactor, and a total gas hourly space velocity (GHSV) of 200,000 h^{-1} was used for the feed stream. The conditions for the Base Case were chosen to represent harsh yet manageable ATR conditions, in terms of carbon deposition and sintering, and such that the produced reformate stream was very near thermodynamic equilibrium under sulfur-free operation. The influence of sulfur under increasingly POX-dominated conditions was studied by considering an elevated atomic oxygen-to-carbon ratio (O/C) and pure POX conditions. Likewise, the role of sulfur in an increasingly SR-dominated environment was studied by an elevated steam-to-carbon ratio (H_2O/C) and under pure SR conditions. For consistency, an inlet temperature of 500 °C was employed for each of the compositions. Since the SR reaction is highly endothermic and has low activity at lower temperatures, the SR experiments were also tested at a feed temperature of 750 °C, in addition to 500 °C.

Assuming that nitrogen is inert under reforming conditions, carbon, oxygen, and hydrogen are the reactive elements in a reformer system (neglecting the relatively low concentration of sulfur and the catalyst material). The balance of these three elements in the design of a reforming system allows for the tuning of carbon deposition behavior, heat duty, product composition, and safe operation. Figs. 1a and b show ternary diagrams for these three elements. Each point on the ternary plot may be taken to represent the elemental balance for a given set of inlet conditions. Tie-lines on the diagram represent the steam reforming of isooctane, the partial oxidation of isooctane, the gasification of elemental carbon, and the desired products of reforming, H_2 and CO (synthesis gas). The bold portion of the partial oxidation line represents the flammability region of isooctane in air at atmospheric pressure.

Open marks in Fig. 1a represent experimental conditions used in previous studies of the effects of sulfur contamination on hydrocarbon reforming [11,16–25]. These studies showed strikingly similar inlet C–H–O compositions employed across a broad range of hydrocarbon fuels (C_7H_{14} to $C_{14}H_{30}$), which can be attributed to a common desire among researchers for low carbon deposition rates, conventionally achieved through high H_2O/C ratios. Only one of the studies chose a feed composition that lay directly on the synthesis gas tie-line [19], the idealized goal of reforming. However, in practical terms that inlet condition was particularly harsh in terms of carbon deposition. The researchers achieved a product stream of almost pure synthesis gas but also reported excessive carbon deposition and sulfur poisoning of their Mo_2C catalyst.

The conditions chosen in this study are depicted in Fig. 1b (closed symbols). The Base Case scenario lies on the edge of the typical operating region for reforming systems, where higher carbon deposition rates are expected. The Elevated H_2O and the Elevated O cases lie on the low and high carbon edges, respectively, of the region most extensively studied in ATR experiments. The Pure POX case lies above the higher flammability limit of isooctane in air and is well within the region where higher carbon deposition rates are expected. The Pure SR case falls on the low H_2O/C side of the region of typical SR experiments.

The ternary diagram was used together with equilibrium calculations to predict the chemical makeup of the product gas. The equilibrium predicted gas compositions were determined for each of the inlet scenarios using the Gibbs free energy minimization method in ASPEN Plus®. For these calculations, the reactor was assumed to be adiabatic, with feed temperatures the same as employed in the experiments (500 °C or 750 °C). The product

Table 1
Reforming scenarios considered. The atomic sulfur concentration refers to the inlet concentration into the reactor.

Scenario	H_2O/C ratio	O/C ratio	$F\_i\text{-}C_8H_{18}$ (mmole/min)	F_H_2O (mmole/min)	F_O_2 (mmole/min)	F_N_2 (mmole/min)	S_0 (ppmv)
Base Case	1	0.75	3.19	25.5	9.56	35.64	4.500
Elevated O	1	1	2.64	21.2	10.58	39.42	3.736
Pure POX	0	0.75	4.85	–	14.55	54.24	6.855
Elevated steam	3	0.75	1.82	45.2	5.47	20.37	2.667
Pure SR	3	0	1.82	45.2	–	25.84	2.667

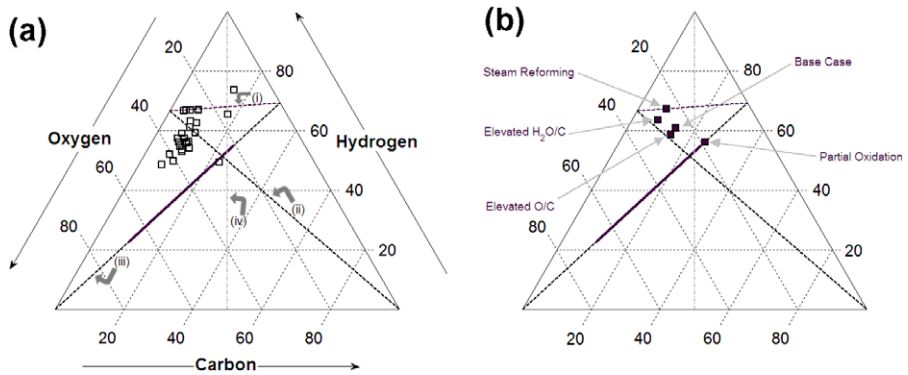

Fig. 1. C–H–O ternary diagrams based on total feed composition. (a) Feed mixtures explored during the investigation of sulfur effects on the reforming of various hydrocarbon feeds [11,40,42,17–24]. (b) Feed mixtures chosen for this study. In Fig. 1a, the line labeled (i) represents the combinations of C_8H_{18} and H_2O (pure SR); likewise, (ii) represents elemental carbon and H_2O; (iii) represents C_8H_{18} and O_2 (pure POX), with the bold portion signifying the flammability region; and (iv) represents synthesis gas compositions.

concentrations of key components for each scenario are listed in Table 2. Based on these calculations, the equilibrium concentration of H_2 in the product stream should follow the trend Base Case > Elevated H_2O > Elevated O > Pure SR (750 °C) > Pure POX > Pure SR (500 °C).

Experimentally, each scenario was independently tested in duplicate under sulfur-free conditions. To determine the influence of thiophene at each set of conditions, each scenario was also independently tested in duplicate using isooctane containing thiophene. The concentration of thiophene in the isooctane stream for these experiments was 77.19 ppmw, corresponding to 29.42 ppmw atomic sulfur. This concentration was selected on the basis of the 2000 Tier 2 Vehicle & Gasoline Sulfur Program Final Rule, which set the EPA guidelines for sulfur content in gasoline. This regulation specifies that the annual average sulfur content of gasoline was not to exceed 30 ppmw for any gasoline producer by the year 2004 [26]. The resulting inlet volumetric concentration of atomic sulfur fed into the reformer at each inlet condition is given in the final column of Table 1. The thiophene concentration in the fuel was verified by means of a Varian Pulsed Flame Photometric Detector (PFPD) installed on a Varian CP-3800 Gas Chromatograph (GC).

2.2.2. Flow reactor description

For each of the reactor experiments, the catalyst was loaded into a 1/2-inch outer-diameter quartz reactor tube where it was supported by coarse-fibered quartz wool. The reactor assembly included a thermocouple shielded within a thermowell, a close-ended 1/8-inch quartz tube. Temperature profiles during the flow experiments were measured by repositioning the thermocouple within the thermowell. The reactor system was loaded into a vertical Thermolyne furnace and was operated in a down-flow configuration. Omega pressure transducers monitored the pressure upstream and downstream of the catalyst bed. The flow system consisted of MKS Flow Controllers for gas delivery and Bronkhorst Liquid Flow Controllers, which controlled Instech peristaltic pumps, for the delivery of liquids. Isooctane and thiophene were obtained from Sigma Aldrich (>99% purity). DI water was used as the steam source. The feed lines were heated to a temperature of 180 °C using Omega heating tape in order to vaporize the liquid feed.

The effluent from the reactor was passed through a single-stage condenser to trap excess water and prevent flooding of the GC columns. The gas phase from the condenser was analyzed using a Varian CP-3800 GC. The lighter components, H_2, O_2, N_2, CO, CH_4, and CO_2, were separated on a HayeSep DIP packed column and quantified using a thermal conductivity detector (TCD). Heavier hydrocarbons, such as ethylene, ethane, propylene, propane, and isobutylene, were separated on an Alltech Carbosphere 1000 packed column and were also quantified using a TCD. Volatile sulfur compounds (VSCs), such as H_2S, methyl mercaptan, and SO_2, were separated on a Restek XLSulfur packed column and analyzed with a Pulsed Flame Photometric Detector (PFPD), whose operation was specifically optimized for atomic sulfur sensitivity and selectivity. The analytical setup also allowed for the detection of isooctane and thiophene in the condenser. However, quantification of these condensable species was indirect because the gas-phase composition of these two chemicals was dependent upon their respective vapor pressures at the condenser operating temperature. For each experiment, the presence or absence of condensable products was noted and the concentration of thiophene was normalized to its steady-state value, providing an estimation of the transient concentration of thiophene.

Stainless-steel lines and related fittings for the entire system were treated with Restek/Silcotek Sulfinert coating, which provided an inert silane surface to the flow path [27–29]. This limited adsorptive losses of VSCs, which is a significant strength of this study [30,31].

Table 2
Predicted exit temperatures and equilibrium gas compositions of key products for the scenarios tested, assuming adiabatic minimization of Gibbs free energy.

Scenario	T (°C)	H_2 (%)	CO (%)	CO_2 (%)	CH_4 (%)	C_2H_4 to C_4H_8 (%)
Base Case	711.39	35.98	15.09	6.71	0.46	0
Elevated O	1003.69	27.43	15.03	4.95	0	0
Pure POX	1108.26	22.00	24.51	0	6.59	0.78
Elevated steam	679.95	30.69	5.30	9.92	0.08	0
Pure SR (500 °C)	407.74	12.18	0.18	6.74	10.58	0
Pure SR (750 °C)	496.54	23.26	1.20	8.49	6.68	0

2.2.3. Reactor startup and shutdown

Prior to reaction, the Ni/CZO catalyst was reduced under a flow of 5% H_2 in N_2 at 600 °C. For the ATR and POX experiments, the catalyst was then cooled under N_2 to an initial reactor temperature of 300 °C. A dual-feed setup allowed the reactant flow to mix and equilibrate before the reaction was initiated. The time at which the flow over the catalyst was switched from N_2 to the reactant stream was taken as the initial time of the experiment. Catalytic light-off occurred immediately upon exposure to the reactant feed in all ATR and pure POX cases and was indicated by a sharp rise in catalyst temperature of at least 100 °C and a slight increase in reactor pressure drop. The furnace temperature was then increased at

10 °C/min to achieve a final reactor feed temperature of 500 °C. It has been reported previously that starting the experiment at a lower initial temperature then ramping to the final feed temperature limits undesirable transient temperature spikes [15]. Air in the ATR and POX experiments was substituted with pure N_2 in the SR experiments, in order to maintain the same space velocity for all experiments. The SR experiments were carried out at a constant furnace set-point of either 500 °C or 750 °C.

The activity and selectivity of the catalyst under each condition was monitored for 500 min. Temperature profiles of the catalyst bed were measured at steady-state conditions. Following each experiment, the catalyst bed was cooled under N_2 flow to help preserve the chemical state of the catalyst. Prior to any post-reaction characterization, the sample was finely ground to thoroughly mix the sample, and thereby minimize sampling error due to inhomogeneity.

2.2.4. Analysis of reforming behavior

The GC quantification provided the dry mole fractions of non-condensable species at a time interval of approximately 35 min. The molar flow-rates, F_X, of each component were calculated using N_2 as an internal standard. These flow-rates were used to calculate the yields for key components (4)–(12). The carbon balance was calculated by summing the yields of carbon-containing products. Under conditions with 100% isooctane conversion, the carbon balance closed to within 5%.

$$Y_{H_2} = \frac{F_{H_2,out}}{9 * F_{C_8H_{18},in}} \quad (4)$$

$$Y_{CO} = \frac{F_{CO,out}}{8 * F_{C_8H_{18},in}} \quad (5)$$

$$Y_{SG} = \frac{(F_{H_2} + F_{CO})_{,out}}{17 * F_{C_8H_{18},in}} \quad (6)$$

$$Y_{CO_2} = \frac{F_{CO_2,out}}{8 * F_{C_8H_{18},in}} \quad (7)$$

$$Y_{CH_4} = \frac{F_{CH_4,out}}{8 * F_{C_8H_{18},in}} \quad (8)$$

$$Y_{2-4} = \frac{(2 * F_{C_2H_4} + 2 * F_{C_2H_6} + 3 * F_{C_3H_6} + 3 * F_{C_3H_8} + 4 * F_{C_4H_8}),out}{8 * F_{C_8H_{18},in}} \quad (9)$$

$$Y_{H_2S} = \frac{F_{H_2S,out}}{F_{C_4H_4S,in}} \quad (10)$$

$$Y_{C_4H_4S} = \frac{F_{C_4H_4S,out}}{F_{C_4H_4S,in}} \quad (11)$$

$$Y_{CH_3S} = \frac{F_{CH_3S,out}}{F_{C_4H_4S,in}} \quad (12)$$

Synthesis gas yield (Y_{SG}) is considered for the purposes of this study to be the most useful single-parameter measure of reforming activity and selectivity. Table 3 shows the Y_{SG} calculated based upon the idealized reaction stoichiometry and the calculated adiabatic equilibrium results. The idealized reaction stoichiometry, as defined in (3) is considered the best possible outcome since the only products considered are H_2 and CO under ATR and SR conditions. These stoichiometrically limited product compositions can also be found using a simple construction using a C–H–O ternary plot, as shown in Fig. 2. A line is drawn between the reactor composition and the point representing pure water. This line will intersect the line representing pure synthesis gas at the constrained dry product gas composition. The stoichiometric limitations of POX are complicated by the sub-stoichiometric oxygen feed requirement for safe operation. The additional carbon in the POX feed was assigned here to ethylene. For all scenarios, equilibrium calculations provide more conservative constraints to Y_{SG} as they consider both the energetic state of the inlet conditions and the presence of undesired products at their thermodynamically favored concentration. In general, the equilibrium calculated Y_{SG} maxima are lower than stoichiometric limited Y_{SG} values due to the presence of compounds such as CO_2 and CH_4 at equilibrium.

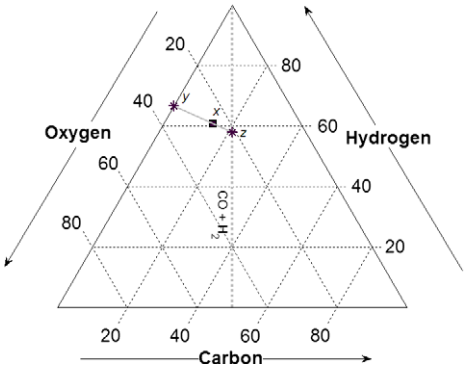

Fig. 2. A C–H–O ternary diagram that shows an example of how to construct a line used to determine the stoichiometric constraint as defined by reaction (3). The line is constructed by connecting the point of pure water (point *y*) with the Base Case inlet conditions (point *x*) and extending the line to intersect with the Syngas line. This intersection (point *z*) represents the ratio H_2/CO for the maximum obtainable Y_{SG}.

2.3. Catalyst characterization

Physical surface area measurement of the prepared catalyst was performed using the single-point BET N_2 physisorption technique on a Quantachrome ChemBET instrument. The metallic surface area and dispersion were determined using H_2 chemisorption on a Micromeritics ASAP 2020 instrument, with the procedure given previously [15].

Gravimetric analyses of temperature-programmed oxidation (TPO) profiles were performed on a TA TGA Q500 instrument. Samples were heated from 100 to 900 °C at 10 °C/min under a flow of 60 mL/min air and 40 mL/min nitrogen to identify and quantify carbon deposited on catalysts during reaction. During this procedure, the oxidation of carbon deposits occurred along with the oxidation of metallic nickel sites. The TPO differential peaks were

Table 3
Idealized stoichiometry for each of the scenarios tested and the maximum theoretical synthesis gas yield obtainable based upon stoichiometric and adiabatic equilibrium calculations.

Scenario	Idealized reaction stoichiometry	Y_{SG} from stoichiometry	Y_{SG} from equilibrium
Base Case	$C_8H_{18} + 2H_2O + 3O_2 \xrightarrow{6H_2O} 11H_2 + 8CO$	1.12	1.08
Elevated O	$C_8H_{18} + 4O_2 \xrightarrow{8H_2O} 9H_2 + 8CO$	1.00	1.00
Pure POX	$C_8H_{18} + 3O_2 \rightarrow 7H_2 + 6CO + C_2H_4$	0.76	0.67
Elevated steam	$C_8H_{18} + 2H_2O + 3O_2 \xrightarrow{22H_2O} 11H_2 + 8CO$	1.12	1.11
Pure SR	$C_8H_{18} + 8H_2O + \xrightarrow{16H_2O} 17H_2 + 8CO$	1.47	0.33 (500 °C) 0.70 (750 °C)

isolated using a deconvolution method. Mass loss peaks occurring between temperatures of 500 and 700 °C were attributed to carbon burn-off. Numerical integration of these peaks provided the mass of the carbon deposited during the reaction.

Powder X-ray diffraction (XRD) was performed on fresh and spent catalysts to identify solid phases present in the sample. The analysis was performed using a Rigaku 12-KW high-intensity rotary anode generator with a Cu K_α source. K_β radiation was filtered with a graphite-diffracted beam monochromator. XRD patterns were analyzed using Jade 9.0 software.

Scanning electron microscopy (SEM) provided visual confirmation of carbon morphologies and the presence of larger Ni particles where applicable. A FEI Nova Nanolab instrument was used to produce micrographs and determine elemental identification and composition calculation using energy-dispersive X-ray spectroscopy (EDS).

3. Results

3.1. Base Case

Fig. 3 shows results for the ATR of isooctane over Ni/CZO with an inlet H_2O/C ratio of 1.0 and an O/C ratio of 0.75. Data are presented for representative sulfur-free and thiophene-exposed experiments. Experimental results were reproducible at all conditions, with variability in the synthesis gas yield (Y_{SG}) of within 1 to 5%. Fig. 3a depicts the Y_{SG} during time-on-stream. The initial time on the *x*-axis is the point at which the catalyst was first exposed to the reactant stream. Fig. 3b shows yields of carbon-containing products (Y_{CO}, Y_{CO_2}, Y_{CH_4}, and $Y_{C_{2-4}}$) averaged over the final three data points of the experiment. The total carbon recovery is given by the sum of these carbon yields. Carbon deposited on the catalyst itself represented a small fraction of the overall carbon and did not significantly influence the carbon balance. Fig. 3c shows the temperature profiles through the reactor collected near the conclusion of each 500-min experiment. The dashed lines show the relative locations of the top and bottom faces of the catalyst bed. Fig. 3d shows the yields of the sulfur species H_2S, thiophene, and methyl mercaptan throughout the duration of the experiment.

When sulfur was not present in the feed stream, the activity of the catalyst was high and stable toward the production of synthesis gas. The carbon balance closed to within 5%, suggesting complete conversion of isooctane, almost entirely to CO and CO_2. The maximum bed temperature was 708 °C with a bed-exit temperature of 676 °C. These reported temperatures are averaged between the repeated experiments. Variability in the bed temperature between repeated experiments was 1–5 °C for most feed scenarios.

When thiophene was present in the feed, both the isooctane conversion and the Y_{SG} were immediately lower than in the sulfur-free case. It is most notable that after the initial loss, the activity remained stable over the course of the experiment. In the presence of sulfur, the carbon balance was skewed noticeably away from CO, and more of the carbon exited the reactor as C_2–C_4 hydrocarbons, especially ethylene, propylene, and isobutylene. The temperature profile of the reactor showed a significantly higher

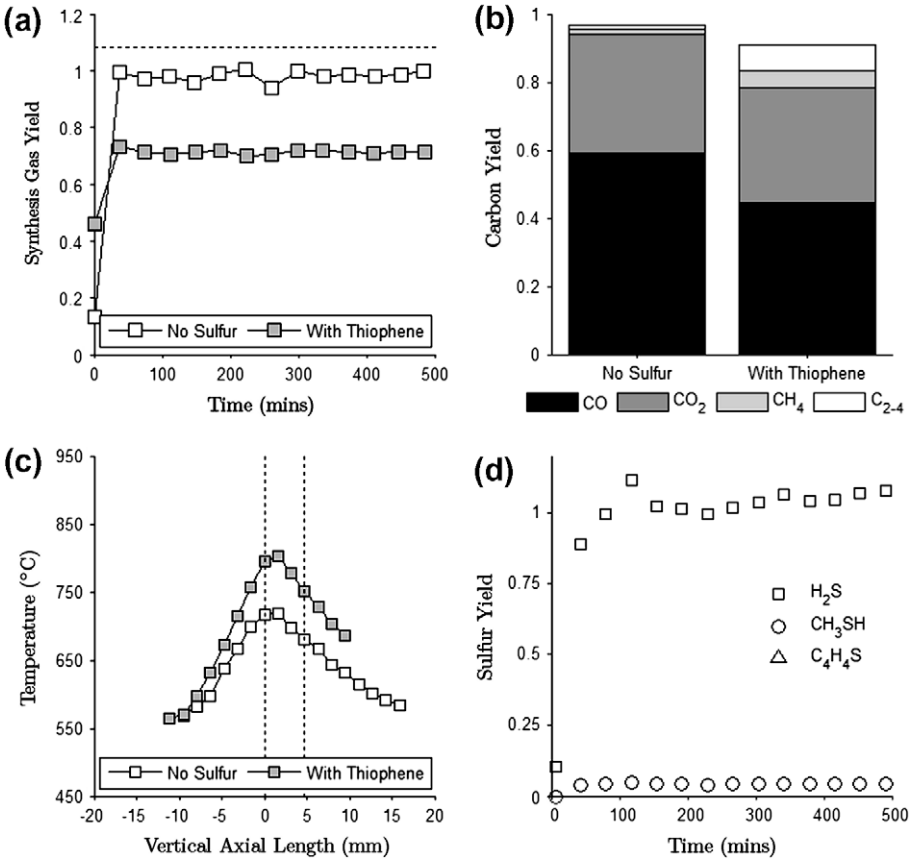

Fig. 3. Results from the Base Case scenario. These panels show the effects of thiophene on Y_{SG} (a), the final yields of carbon species (b), and the steady-state axial reactor temperature profile (c). The dashed line in (a) shows the equilibrium predicted Y_{SG} (see Table 3). The dashed lines in panel (c) show the best approximation of the catalyst bed location, with negative axial length values denoting upstream temperatures and positive values for distance below the front face of the catalyst. Panel (d) shows the yield of major sulfur components in the product stream when thiophene is present in the Base Case. (Reactor conditions: H_2O/C = 1, O/C = 0.75, GHSV = 200 k h^{-1}, T_{inlet} = 500 °C, S_{in} = 0 or 4.5 ppmv.)

catalyst bed temperature compared to the Base Case without sulfur. In this experiment, the maximum bed temperature was 798 °C and the temperature at the bottom face of the catalyst bed was 778 °C. Breakthrough of sulfur occurred within the first 10 min-on-stream, and the atomic sulfur balance could be closed within the first 100 min-on-stream. Thiophene was almost entirely converted to H_2S with less than 10% of the sulfur yielded as methylmercaptan.

3.2. Elevated O scenario

The influence of thiophene on reforming behavior for feed conditions with an elevated oxygen concentration (O/C = 1, H_2O/C = 1) is shown in Fig. 4. Without the presence of sulfur, the composition of carbon species was similar to the Base Case although there was a slightly lower Y_{SG} due to lower H_2 production. The temperature profile through the reactor showed significantly higher peak (822 °C) and bed-exit (807 °C) temperatures than the Base Case.

In the Elevated O case, the presence of thiophene had a markedly different effect upon reforming behavior when compared to the Base Case. Initial selectivity toward synthesis gas was similar to sulfur-free conditions, but decreased over time in a trend suggesting continual deactivation. Carbon product yields in this case were almost evenly weighted between CO, CO_2, and the C_2–C_4 hydrocarbons, which were primarily olefins. The temperature profile showed that the reactor was again hotter in the presence of thiophene, although this heat effect was less pronounced than was seen in the Base Case. The maximum bed temperature in this experiment was 842 °C and the bed-exit temperature was 829 °C. In contrast to the Base Case, the thiophene was not completely converted to H_2S. After an initial partial conversion to H_2S and methylmercaptan, within 200 min-on-stream, only thiophene was seen exiting the reactor.

3.3. Pure POX scenario

The results of extending the influence of O concentration to pure POX conditions, with an O/C ratio of 0.75, are shown in Fig. 5. The activity was significantly lower than in the Base Case or the Elevated O case, even under sulfur-free conditions. However, the Y_{SG} was relatively stable over the course of this experiment, approximately 40%. The POX conditions resulted in a high CO/CO_2 ratio along with a significant level of olefins in the product stream. The sulfur-free maximum bed temperature was 790 °C, and the temperature at the bottom of the catalyst bed was 772 °C.

With thiophene present in the isooctane feed, the consequences on Y_{SG} were similar to the Elevated O scenario, with an initial value similar to the sulfur-free experiment quickly showing a steady decline. Unlike the other feed conditions, there was no significant loss of isooctane conversion due to the presence of thiophene. However, a large portion of the carbon exited the reactor in the form of propylene and isobutylene. Reactor temperature measurements showed that the presence of thiophene coincided with a significant increase in reactor bed temperature with a peak temperature of 919 °C and a temperature at the base of the catalyst bed of 901 °C. Temperature measurements between the duplicated experiments showed significantly higher variability compared to other feed scenarios. The standard deviations of the experiments were 23 °C and 36 °C for the maximum bed and the bed-exit temperatures, respectively. Similar to the Elevated O scenario, thiophene

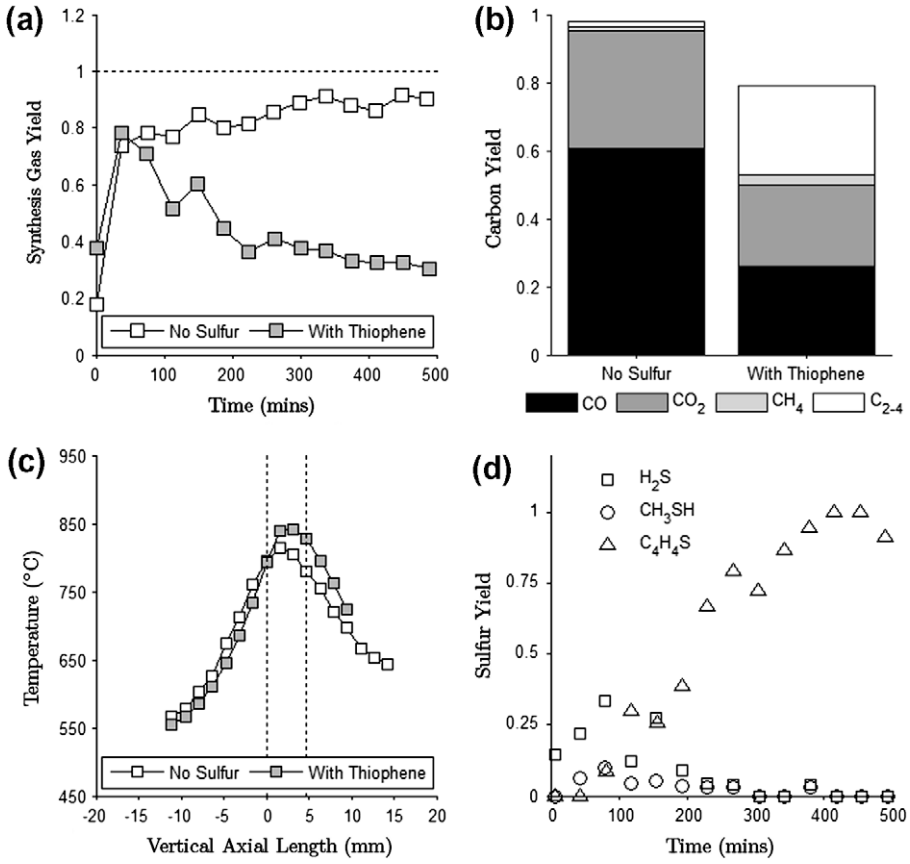

Fig. 4. Results from the high O scenario. (a) Y_{SG} as a function of time-on-stream, (b) final yields of carbon species, (c) axial temperature profiles, and (d) yields of sulfur species. (Reactor conditions: H_2O/C = 1, O/C = 1, GHSV = 200 k h^{-1}, T_{inlet} = 500 °C, S_{in} = 0 or 3.7 ppmv.)

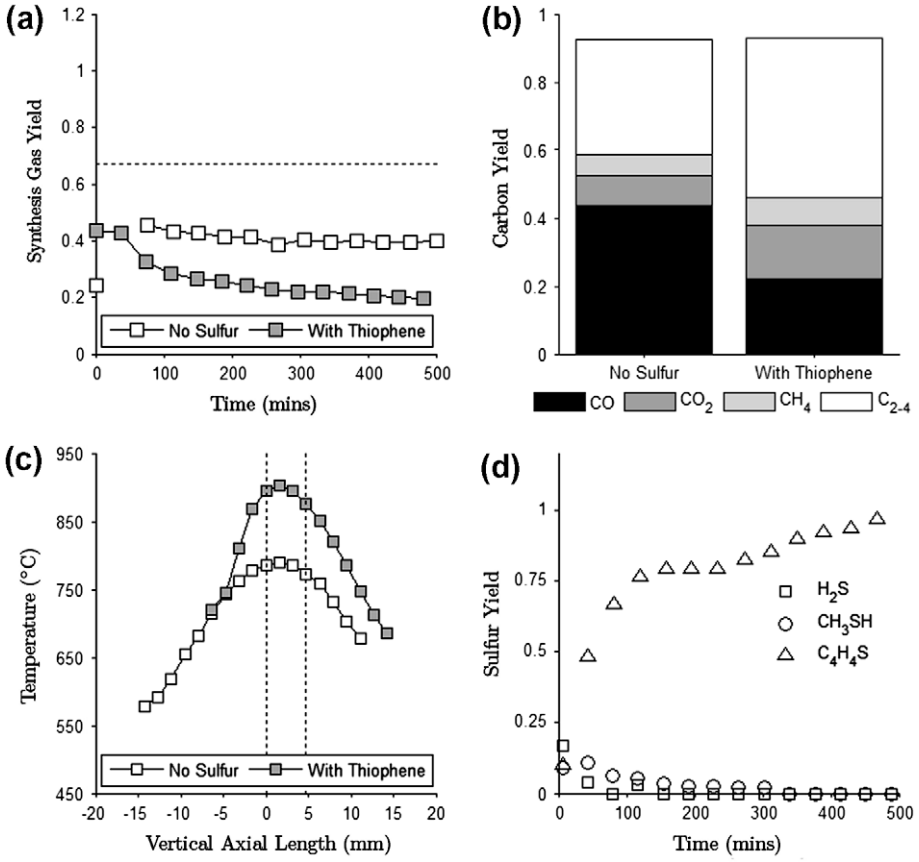

Fig. 5. Results from the pure POX scenario. (a) Y_{SG} as a function of time-on-stream, (b) final yields of carbon species, (c) axial temperature profiles, and (d) yields of sulfur species. (Reactor conditions: $H_2O/C = 0$, $O/C = 0.75$, GHSV = 200 k h^{-1}, $T_{inlet} = 500$ °C, $S_{in} = 0$ or 6.9 ppmv.)

was only initially converted to methylmercaptan and H_2S, and eventually unreacted thiophene was the only sulfur-containing component in the product stream.

3.4. Elevated H_2O scenario

Results of the Elevated H_2O feed experiments ($O/C = 0.75$, $H_2O/C = 3$) are shown in the panels of Fig. 6 and closely resemble the results of the Base Case. Under sulfur-free conditions, the Y_{SG} was high and stable, about 90%. The carbon balance indicated only about a 90% conversion of isooctane. The reaction more strongly favored the production of CO_2 than the experiments with lower concentrations of H_2O. However, almost no methane was seen in the exit stream and C_2–C_4 hydrocarbons were not detected. The maximum temperature for this experiment was 685 °C, and the temperature at the lower face of the catalyst was 665 °C.

With the presence of thiophene, the isooctane conversion was lower and the Y_{SG} was diminished but stable, and production of isobutylene and propylene occurred. As in the other scenarios, the temperature in the reactor was higher. The maximum temperature was 745 °C, and the bed-exit temperature was 734 °C. Thiophene was completely converted to H_2S at steady-state.

3.5. Pure SR scenario

Ni/CZO was not found to be significantly active under SR conditions ($H_2O/C = 3$) at the inlet temperature of 500 °C (Fig. 7). However, a small hydrogen yield was fairly stable over the course of the experiment, with less than 10% conversion of isooctane to CO_2. However, when thiophene was added to the fuel, the minimal reforming activity vanished within the first 30 min of the experiment, and thiophene emerged as the only sulfur product from the reactor. The sulfur-free SR activity was significantly higher for an inlet temperature of 750 °C. But again, the presence of thiophene led to a complete loss of activity in the first 30–90 min of the experiment.

3.6. Carbon deposition during reforming

Average carbon deposition rates for the reforming experiments are shown in Table 4. TPO analysis showed that carbon deposition rates were below detectable limits for all Elevated O and Elevated H_2O experiments, and for the 500 °C SR with thiophene experiment. Two broad mass gain peaks at 400 °C and 550 °C are due to the oxidation of metallic nickel. The mass loss peaks, attributed to carbon oxidation, occur over a range of temperatures between 500 and 700 °C. The lowest quantifiable carbon deposition rate is approximately 0.3 mg C/(g catalyst $*$ h) as small mass loss peaks cannot be distinguished from the mass gain peaks associated with Ni oxidation.

The carbon deposition rate data show that there was significantly more carbon deposited during the POX experiments than during the ATR or SR experiments. Conclusions regarding the effect of thiophene upon carbon deposition were difficult to deduce based on the data of Table 4. The presence of thiophene under Base Case and 500 °C SR conditions coincided with lower carbon present on post-reaction samples than after sulfur-free experiments. Conversely, carbon deposition was more pronounced under thiophene exposure during POX experiments and the 750 °C SR conditions. However, these differences are all within the experimental error of the analysis and are not significant trends. Overall, the carbon

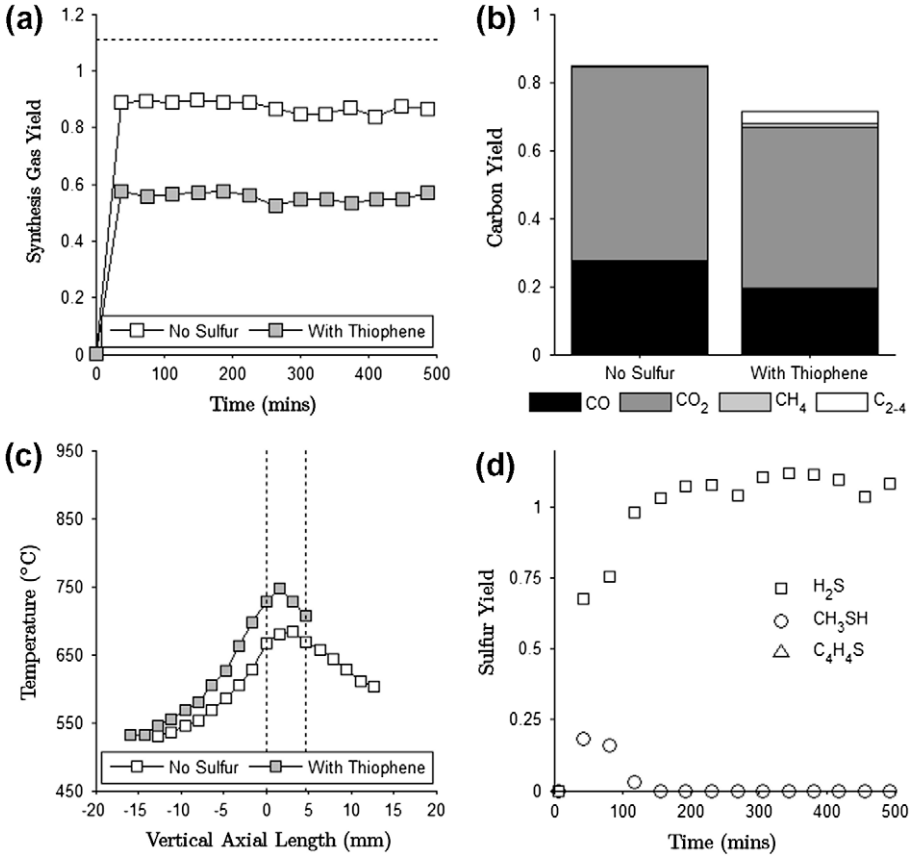

Fig. 6. Results from the elevated H_2O scenario. (a) Y_{SG} as a function of time-on-stream, (b) final yields of carbon species, (c) axial temperature profiles, and (d) yields of sulfur species. (Reactor conditions: $H_2O/C = 3$, $O/C = 0.75$, GHSV = 200 k h^{-1}, $T_{inlet} = 500$ °C, $S_{in} = 0$ or 2.7 ppmv.)

deposition rates for all but the most extreme POX conditions were relatively low.

The morphologies of the carbon deposits were analyzed using SEM, and Fig. 8 shows representative images. Fig. 8a shows the structure of the reduced catalyst prior to reaction. All samples exposed to ATR conditions, regardless of exposure to thiophene, had structures like those seen in Fig. 8b, which shows a micrograph of the post-reaction sample from the Base Case scenario with thiophene. Large particles of Ni with diameters between 50 and 500 nm were visible in all post-reaction samples, except those of SR experiments. Carbon deposits generally take the form of coating or encapsulating deposits or filament-like structures [12]. There were no carbon filaments visible in any ATR post-reaction samples, suggesting the formation of only coating-types of carbon.

Carbon filaments of various diameters were seen in POX post-reaction samples and SR samples not exposed to thiophene. Fig. 8c shows the catalyst after reaction under POX conditions without sulfur. This image shows a region of high carbon filament concentration with diameters ranging between 40 and 150 nm. Ni particles as large as 500 nm are visible as well as regions of almost pure CZO. Fig. 8d shows the effect of thiophene on carbon morphologies formed under POX conditions. The top portion shows a large carbon filament (~350 nm), representative of the majority of carbon structures found throughout the sample. The bottom portion shows a particle of pure carbon presumably formed through the coalescence of large carbon filaments.

3.7. Surface area measurements

The physical surface area of the CZO support alone was 18.71 m^2/g and the surface area of the Ni/CZO catalyst was 13.94 m^2/g, as determined by single-point BET N_2 physisorption. H_2 chemisorption on reduced Ni/CZO was performed to determine the availability of active metal sites. The metal dispersion of the fresh catalyst was 1.69%, and the active metal surface area was 1.12 m^2/g catalyst. Fig. 9 shows chemisorption results from samples after reaction at each condition. These samples were reduced prior to chemisorption. In all experiments, a significant fraction of hydrogen uptake capacity was lost. The decrease in hydrogen chemisorption uptake was even more pronounced in cases with thiophene exposure. For example, at the Base Case conditions, the presence of thiophene resulted in a 37% less hydrogen uptake. The most pronounced effect of thiophene was under POX conditions, where the hydrogen uptake was 81% lower when thiophene was present compared to sulfur-free POX runs. In the SR case, where the sulfur-free activity was low and the activity under thiophene exposure was undetectable, there was a 40% decrease in hydrogen uptake after reaction without sulfur and an 87% decrease after thiophene contaminated conditions.

3.8. XRD measurements

Selected results from the powder XRD analysis are shown in Fig. 10. The XRD patterns for the CZO support and for fresh reduced Ni/CZO are shown at the bottom of the figure. The catalyst showed reflections for both CeO_2 and metallic Ni. The CeO_2 reflections were shifted slightly to higher 2θ values than reported in the literature, consistent with inclusion of Zr in the Ce lattice [40]. Furthermore, in several of the samples there is a pronounced shoulder visible at the CeO_2 reflection in the region of $2\theta = 26–32°$. Recent work has shown that these discrepancies between CeO_2 and CZO reflections are due to separate phases of higher relative Ce and Zr concentra-

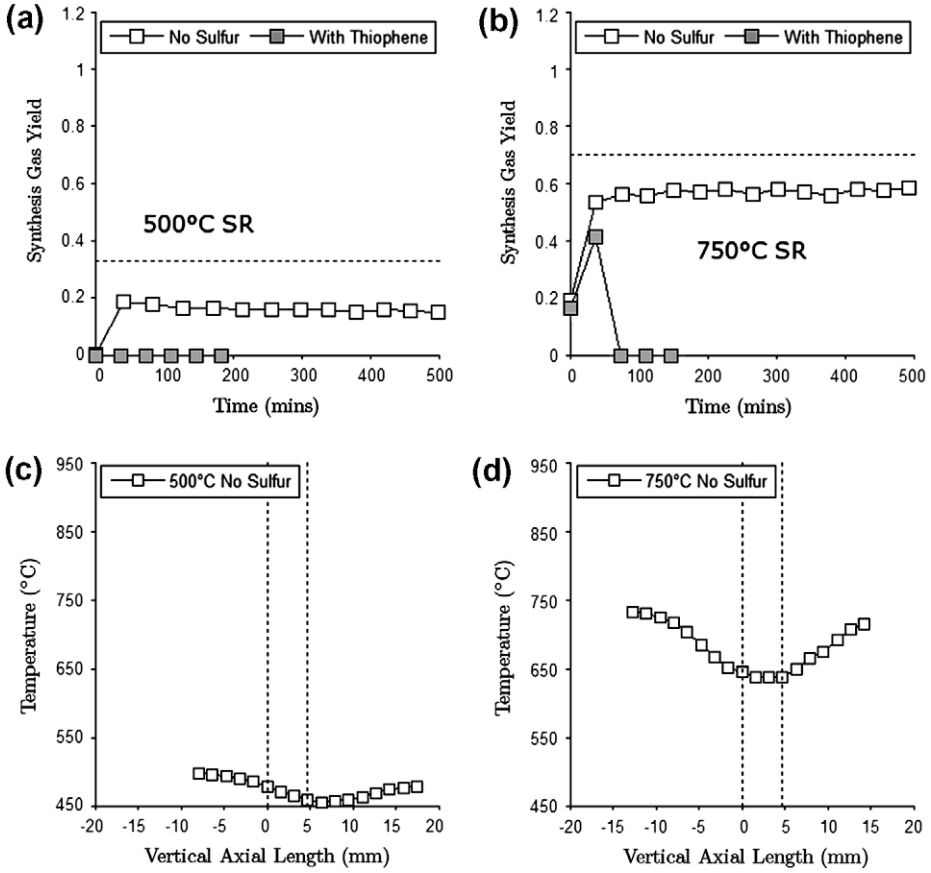

Fig. 7. Results from the pure SR scenarios. (a) Effect of thiophene on Y_{SG} under SR at an inlet temperature of 500 °C, (b) effect of thiophene on SR activity with an inlet temperature of 750 °C, and (c and d) steady-state axial temperature profiles for SR at 500 °C and 750 °C, respectively. (Reactor conditions: $H_2O/C = 3$, $O/C = 0$, GHSV = 200 k h^{-1}, T_{inlet} = 500 °C or 750 °C, S_{in} = 0 or 2.7 ppmv.)

Table 4
Carbon deposition rates as determined by TPO, mg C/(g catalyst h).

Reforming scenario	No sulfur	With thiophene
Base Case	7.59 ± 7.38	0.82 ± 0.53
Elevated O	⩽0.3	⩽0.3
Pure POX	81.16	102.17 ± 54.35
Elevated H_2O	⩽0.3	⩽0.3
Pure SR (500 °C)	5.33 ± 3.31	⩽0.3
Pure SR (750 °C)	59.85	61.05

tions [32]. Representative XRD patterns for post-reaction samples are also shown in Fig. 10. In all cases, the nickel reflections were stronger following reaction when compared to the fresh sample. These reflections were weaker for thiophene-exposed samples than they were for sulfur-free samples. The high carbon deposition rates of the POX experiments coincided with the presence of graphitic reflections in post-reaction samples. NiO reflections were only visible for the post-ATR Elevated H_2O samples.

4. Discussion

The influence of sulfur on Ni-based catalysts has attracted interest due to the implications for the industrial steam reforming and hydrodesulfurization processes [33,34]. Studies on model systems have shown that the adsorption of sulfur on various crystallographic planes of Ni at high coverages provides the thermody-

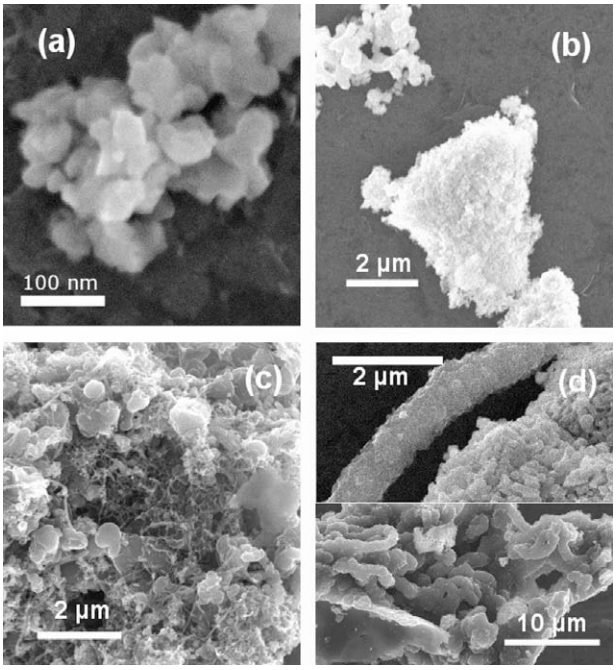

Fig. 8. (a) SEM image of a fresh, reduced 10 wt.% Ni/CZO catalyst. (b) SEM image of a post-reaction catalyst following Base Case conditions with thiophene. (c) Carbon filament domains for a catalyst after POX without sulfur. (d) Carbon morphologies of POX sample exposed to thiophene.

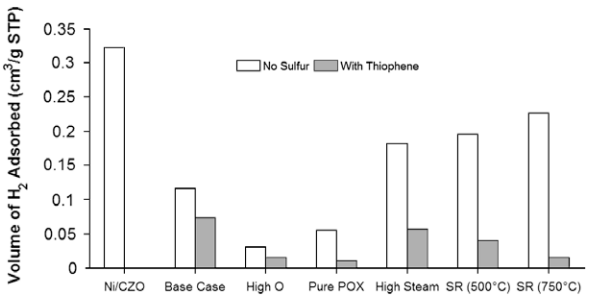

Fig. 9. H_2 uptake of catalyst prior to reaction and after reaction at each condition.

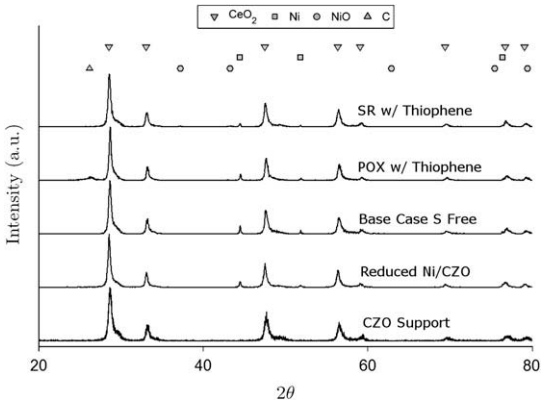

Fig. 10. X-ray diffraction patterns of CZO support, reduced Ni/CZO catalyst and representative post-reaction samples. Reference reflections are shown above the figure [43–45].

namic driving force for surface restructuring, leading to profound changes in activity and selectivity [35,36]. Charge transfer from metal *d*-orbitals to sulfur-localized orbitals during the formation of surface-bound sulfides leads to a decrease in the chemisorption activity of the metal [13]. The extent of this interaction is dependent upon several factors including sulfur concentration, exposure time, and various catalyst properties.

The lack of a thorough appreciation of the role of sulfur in an ATR reactor is primarily a consequence of the complex nature of this system. One may visualize an autothermal reformer as consisting of three distinct regions with significantly different reactive environments. In the first region, radiative heat transfer from the catalyst provides the thermal energy for homogeneous decomposition and oxidative cracking of hydrocarbons, producing CO and lighter hydrocarbons. Molecular oxygen is then rapidly depleted in a shallow front-section of the catalyst bed through fast and exothermic catalytic partial oxidation and total oxidation reactions. The majority of the catalyst bed is dominated by slower reactions such as the highly endothermic reforming of light hydrocarbons and the establishment of thermodynamic equilibrium, presumably through a water gas shift mechanism. This depiction has been developed explicitly for POX systems using spatially resolved techniques [37] and has been implicitly extended to describe ATR systems [38,10,39,40].

The experiments in this study have been performed in order to describe the behavior of thiophene under various reforming conditions. Under all reaction conditions, the presence of thiophene resulted in an elevated reactor temperature and diminished selectivity toward synthesis gas production. Furthermore, more of the carbon exited the reactor in the form of hydrocarbons, especially propylene and isobutylene. These olefins are mostly formed through a homogeneous thermal cracking mechanism and are consumed by catalytic steam reforming. Their increased concentration under thiophene exposure may therefore be attributed to diminished steam reforming activity. This diminished activity toward endothermic mechanisms is consistent with the elevated catalyst bed temperature.

In order to gain further insight into the reforming behavior, equilibrium calculations were performed using ASPEN. The equilibrium composition was calculated by minimizing the Gibbs free energy at the measured temperature and pressure at the end of the catalyst bed (unlike the preliminary results given in Table 2 that assumed adiabatic behavior). Thermodynamic calculations offer a convenient way to contextualize the results of reforming experiments. Table 5 shows how the measured outlet compositions of each experiment compared to equilibrium at the exit temperature and pressure. Thermodynamic equilibrium is effectively the reactor-exit composition at infinite residence time. Thus, deviations from equilibrium compositions give a clue to the relative contributions of various reaction mechanisms and particularly provide insight into which reactions were incomplete. For example, the positive deviation of CO_2 concentration for all experiments suggests that mechanisms leading to CO_2 formation, such as catalytic total oxidation, have lower overall activation barriers than mechanisms resulting in CO_2 depletion, such as reverse water gas shift and dry reforming.

Under sulfur-free conditions, the data in Table 5 demonstrate that product compositions are very near thermodynamic equilibrium for all feed conditions except for SR, where low methane production resulted in a significant positive H_2 deviation. In all scenarios, the presence of thiophene led to more pronounced positive, or less negative equilibrium deviations for CO_2, CH_4, and C_2–C_4 hydrocarbons and more pronounced negative deviations for H_2 and CO. This suggests that the mechanisms leading to light hydrocarbon reforming and CO_2 depletion are most adversely affected by the presence of thiophene, especially under conditions of high oxygen feed.

Table 5
Measured average product mole composition (no N_2, *i*-C_8H_{18} or H_2O) compared to equilibrium predicted molar composition. Equilibrium values (given in parentheses) were calculated at the measured temperature of the bottom face of the catalyst.

Experimental condition	H_2	CO	CO_2	CH_4	$\sum C_2H_4$ to C_4H_{10}
Base Case no sulfur	60.5% (60.9%)	24.1 (23.9)	14.4 (13.1)	0.97 (2.03)	0.02 (9.94E−6)
Base Case with thiophene	56.5 (61.9)	23.0 (28.0)	17.4 (9.9)	2.09 (0.14)	0.93 (2.81E−7)
Elevated O no sulfur	55.7 (59.2)	27.7 (27.4)	15.1 (13.4)	0.88 (0.03)	0.66 (2.58E−8)
Elevated O with thiophene	39.3 (59.0)	27.4 (27.9)	24.4 (13.0)	3.40 (0.02)	5.46 (1.5E−8)
POX case no sulfur	38.4 (38.3)	40.8 (46.1)	7.55 (0.09)	5.90 (15.6)	7.40 (0.007)
POX case with thiophene	17.7 (38.7)	30.2 (46.1)	14.4 (0.002)	14.0 (15.1)	22.8 (0.14)
Elevated H_2O no sulfur	64.2 (66.8)	11.8 (11.1)	23.6 (21.9)	0.39 (0.26)	*Below detection* (1.44E−7)
Elevated H_2O with thiophene	59.6 (66.4)	11.2 (13.1)	28.3 (20.5)	0.59 (0.05)	0.34 (1.33E−8)
SR case no sulfur (500 °C)	75.6 (54.8)	1.21 (2.14)	23.1 (22.0)	0.03 (21.1)	0.03 (0.008)
SR case with thiophene (500 °C)	N/A	N/A	N/A	N/A	N/A
SR case no sulfur (750 °C)	70.6 (71.4)	8.28 (11.5)	15.3 (15.4)	2.63 (1.61)	3.16 (3.28E−8)
SR case with thiophene (750 °C)	N/A	N/A	N/A	N/A	N/A

Stoichiometric considerations also aid in understanding the role of separate reaction mechanisms. Fig. 1b shows the position of the reaction conditions on a ternary diagram. Considering the atomic balance of H, O, and C in the reactor provides a way to manage certain key system processes. For example, as demonstrated in this study, the Elevated H_2O and Elevated O feed scenarios both showed minimal carbon deposition and also produced less-negative deviations of CO from equilibrium in the presence of thiophene. These effects may be due to a greater availability of atomic oxygen, either from higher H_2O or O_2 feed. More molecular oxygen in the feed leads to a greater importance of oxidative cracking, a production route for CO. Similarly, the higher availability of atomic oxygen leads to an increased ability to remove carbon from the catalyst surface.

An important distinction of this study lies in endeavors to identify and quantify sulfur products leaving the reformer. A common assumption has been that thiophene and other VSCs are completely converted to H_2S immediately in the catalyst bed. It is true that under all reforming conditions, there is a large thermodynamic driving force toward H_2S formation. However, this study has demonstrated for the first time that the hydrodesulfurization (HDS) performance of nickel is related to its reforming activity. HDS of thiophene is a two-step process in which thiophene is first adsorbed and hydrogenated on a nickel site leading to a nickel–sulfide bond, and then the blocked site is 'cleaned' by chemisorbed hydrogen leading to the formation of H_2S [41].

It has been proposed that the rate of HDS is proportional to the number of vacant Ni sites, which is in turn dependent on both the strength of the Ni–S bonds and the composition of the vapor phase [39]. The thiophene conversion should therefore be closely linked to the availability of hydrogen to both hydrogenate chemisorbed thiophene and to 'clean' sulfided nickel sites. As seen in the results of Table 2, there is a correlation between the equilibrium partial pressure of hydrogen and tolerance to thiophene during reforming over nickel. In particular, the Base Case and Elevated H_2O experimental conditions showed both sustained activity under the presence of thiophene and the highest equilibrium H_2 partial pressures.

Based on these observations, it is proposed that when the HDS process proceeded normally, only the most active steam reforming sites were blocked by sulfur, and sulfur coverage quickly reached equilibrium. Consequently, a diminished yet stable steam reforming activity persisted over time, which resulted in elevated catalyst bed temperatures and a lower synthesis gas production when compared to sulfur-free operation. Conversely, when this low sulfur-coverage equilibrium was not reached, perhaps due to a lower availability of surface-bound hydrogen, site-blocking sulfides accumulated on even the less active nickel sites and thereby caused a continuous drop in activity over time.

The relationship between equilibrium hydrogen composition and sulfur tolerance was developed in this study for five specific inlet conditions. Fig. 11 provides a predictor of performance over a broader range of reforming conditions. The results of adiabatic Gibbs free energy minimization calculations are shown for H_2O/C from 0 to 10 and O/C from 0 to 2. Fig. 11a shows a contour plot of adiabatic reactor temperatures on a C–H–O ternary diagram and Fig. 11b shows the H_2 equilibrium mole fraction. Fig. 11a demonstrates that as the O/C ratio increases above one, the equilibrium temperature begins to increase into an undesired region, both in terms of catalyst sintering and in terms of safe operation. Fig. 11b provides an implicit prediction of the tolerance of the reforming system to thiophene exposure. Based upon the results of this study, equilibrium hydrogen compositions above 28% (the two lighter shaded regions in Fig. 11b) are associated with both high HDS activity and stable performance under thiophene exposure. It would be advantageous to construct a similar map describing carbon deposition behavior to further define optimal reformer inlet conditions.

Thiophene exposure also has an impact on the structure of the catalyst. Particle agglomeration is unfavorable as this decreases the availability of active surface sites. While it would be reasonable to assume that the elevated bed temperature experienced under thiophene exposure would have increased the rate of particle growth, the results from this study do not show a conclusive relationship between thiophene exposure and rates of sintering. Both SEM and chemisorption results suggested an increase in particle size after sulfur exposure; however, XRD results implied the opposite as the presence of thiophene led to a decrease in the intensity of Ni reflections. The reconciliation of these observations is not possible at present due to the limitations of the characterization techniques used. For example, the hydrogen uptake during the chemisorption analysis may be underestimated due to the presence of surface-bound sulfur atoms. Visual confirmation of particle size using SEM suffers from large sampling error leading to a bias toward larger particles. XRD results also provide an incomplete description of the bulk structure due to several sources of uncertainty, including intra-particle grain boundaries, amorphous Ni regions, and low concentration or small particles of bulk nickel sulfide.

The identification of sulfur species on the post-reaction catalyst samples was attempted, with mixed results. XRD analysis did not show any sulfide or sulfate phases in any of the thiophene-exposed samples. The sulfur 2p, 2s, and LMM auger transition regions were

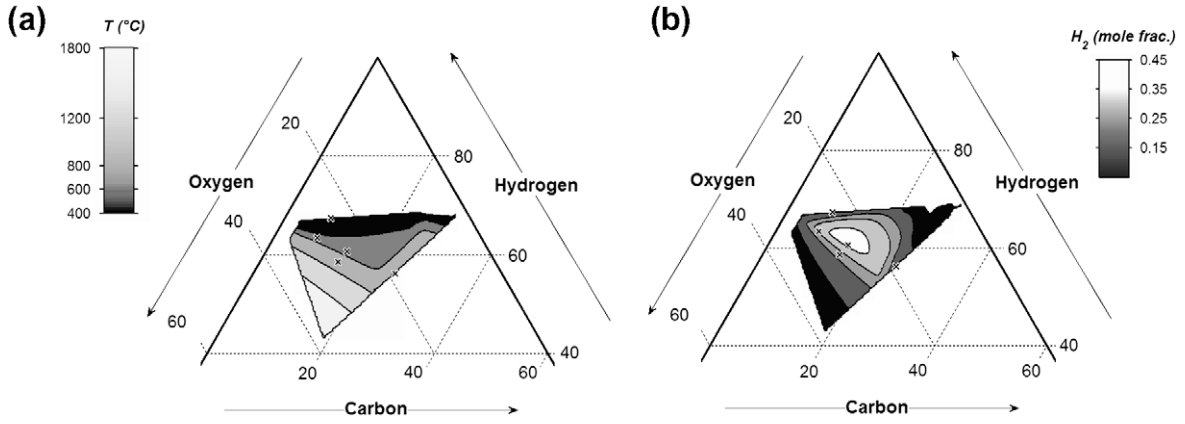

Fig. 11. Contour plots of adiabatic exit temperature (a) and H_2 mole fraction (b) over the C–H–O space calculated by Gibbs free energy minimization of isooctane reforming. H_2O/C ratios ranged from 0 to 10 and O/C ratios ranged from 0 to 2. The equilibrium calculations were performed in ASPEN using isooctane, water and air as reactants with feed temperature of 500 °C. In both diagrams, the 'x' marks show the conditions considered in this study.

Table 6
Atomic ratio of sulfur to nickel calculated from the breakthrough of sulfur-containing species from the reactor using expression (13).

Reforming scenario	S/Ni ratio calculated from *S* breakthrough
Base Case with thiophene	0.01364
Elevated O with thiophene	0.04118
Pure POX with thiophene	0.02620
Elevated H_2O with thiophene	0.01143
Pure SR with thiophene (500 °C)	0.00489
Pure SR with thiophene (750 °C)	N/A

scanned by X-ray photoelectron spectroscopy (XPS) for all samples to identify sulfur species on the surface of the catalyst. However, positive identification of sulfur was not achieved, possibly due to the low signal-to-noise ratio for these transitions. EDS measurements of SEM micrographs showed that sulfur was present on the Elevated Oxygen post-reaction sample. In this case, sulfur was only detected in regions of high Ni concentration, suggesting that sulfur was in close contact with nickel, supporting the theory that thiophene exposure at these conditions was responsible for loss of active nickel sites. The ability to identify and quantify sulfur from EDS measurements was complicated by the presence of the overlapping zirconium peak.

An approximation can be made as to the sulfur content of post-reaction samples by analyzing the breakthrough curves of sulfur species through the reactor. Eq. (13) gives the expression used to approximate the ratio of sulfur atoms to Ni atoms in the post-reaction sample.

$$\mathrm{S:Ni} = \frac{F_{\mathrm{thiophene,in}}}{\mathrm{cat\ mass} * \mathrm{Ni\ loading}/\mathrm{MW_{Ni}}} \times \sum_t \left\{\left(1 - Y_{\mathrm{H_2S}} - Y_{\mathrm{CH_3S}} - Y_{\mathrm{C_4H_4S}}\right) \cdot \Delta t\right\} \quad (13)$$

The results for each reforming scenario are given in Table 6. The values given in Table 6 likely suffer from a small systematic error due to unavoidable adsorptive losses of VSCs in the condenser. However, since this error is constant for all experiments, the trends shown in Table 6 are valid. As confirmed by SEM, the Elevated O scenario led to the most sulfur present on the catalyst. Such high adsorption levels of sulfur may have led to a loss in catalytic POX activity as well as SR activity, which may explain why the temperature rise due to the presence of thiophene was least severe under these conditions. The comparatively lower sulfur accumulation at pure POX conditions suggests that the excessive carbon deposition and sulfur blocking of steam reforming sites played a combined role in the poor selectivity toward synthesis gas production at these conditions.

Under the Base Case and Elevated H_2O ATR experiments, and the pure SR experiments, analysis of sulfur breakthrough showed less accumulation of sulfur compared to the Elevated O and pure POX feed conditions, despite their cooler bed temperatures. This observation is counterintuitive based on the inverse temperature dependence of the sticking coefficient. Low sulfur capacity under the two ATR conditions may be due to high HDS activity facilitated by high availability of H_2. The fact that the SR activity of the catalyst was completely diminished in the presence of thiophene suggests that the reforming activity under thiophene-free conditions was owed to the most highly active sites, which were also the most susceptible to site blockage by adsorbed sulfur species.

5. Conclusions

In this study, the effects of thiophene on the isooctane reforming activity of $Ni/Ce_{0.75}Zr_{0.25}O_2$ catalysts were investigated under conditions representing five separate points on the C–H–O ternary diagram. These conditions ranged from pure SR to pure POX, with the intermediary points representing typical autothermal reforming O/C and H_2O/C ratios.

It has been convincingly shown that adding even small amounts of thiophene to POX and ATR reformer feed streams can drastically alter the temperature profile in the reactor, leading to significant increases in catalyst bed temperatures. These temperature increases suggest that sulfur selectively blocks Ni sites responsible for endothermic steam reforming reactions, while having less effect on the sites responsible for exothermic partial or total oxidation reactions.

Remarkably, the reactivity of thiophene depends strongly on the reaction conditions. Depending upon the feed conditions, either the complete conversion of thiophene to H_2S or the breakthrough of unreacted thiophene was observed. The latter case coincided with a continuous decline in reforming activity over time-on-stream. In cases where complete conversion to H_2S occurred, an immediate but modest decrease in activity was observed, followed by stable reforming performance thereafter. Under pure steam reforming conditions, thiophene exposure caused complete deactivation of the catalyst and thiophene emerged unconverted. This work has shown that certain reaction conditions can be selected that maximize the availability of H_2 and that these conditions govern both the reforming stability and the conversion of thiophene to H_2S. This offers a promising strategy for maintaining reforming activity in the presence of sulfur compounds.

Acknowledgments

The authors would like to acknowledge the financial support provided by the US Army Tank-Automotive Research, Development and Engineering Center under Cooperative Agreement Number W56HZV-05-2-0001 and by the US Department of Energy under Contract Number DE-FC26-06NT42813. The authors thank the Electron Microbeam Analysis Laboratories (EMAL) of the University of Michigan for providing access to SEM instruments through the support of NSF Grant No. DMR-0320740. Jonathon Butler performed some of the TPO and H_2 chemisorption post-reaction characterization. Ternary plots were prepared based on the code, Ternplot, shared by Carl Sandrock at the MATLAB Central File Exchange (http://www.mathworks.com/matlabcentral/fileexchange/2299).

References

[1] M. Krumpelt, T. Krause, J. Carter, J. Kopasz, S. Ahmed, Catal. Today 77 (2002) 3.
[2] R. Navarro, M. Álvarez-Galván, F. Rosa, J. Fierro, Appl. Catal. A 297 (2006) 60.
[3] L. Pino, A. Vita, F. Cipitì, M. Laganà, V. Recupero, Appl. Catal. A 306 (2006) 68.
[4] H. Koga, S. Fukahori, T. Kitaoka, A. Tomoda, R. Suzuki, H. Wariishi, Appl. Catal. A 309 (2006) 263.
[5] S. Barison, M. Battagliarin, S. Daolio, M. Fabrizio, E. Miorin, P. Antonucci, S. Candamano, V. Modafferi, E. Bauer, C. Bellitto, G. Righini, Solid State Ionics 177 (2007) 3473.
[6] M. Nilsson, P. Jozsa, L. Pettersson, Appl. Catal. B 76 (2007) 42.
[7] M. Fytzani-Stephanopoulos, G. Voecks, Int. J. Hydrogen Energy 8 (1983) 539.
[8] K. Nagaoka, K. Takanabe, K. Aika, Appl. Catal. A 268 (2004) 151.
[9] J. Sehested, Catal. Today 111 (2006) 103.
[10] N. Laosiripojana, S. Assabumrungrat, Appl. Catal. A 290 (2005) 200.
[11] D. Shekhawat, T. Gardner, D. Berry, M. Salazar, D. Haynes, J. Spivey, Appl. Catal. A 311 (2006) 8.
[12] X. Chen, A. Tadd, J. Schwank, J. Catal. 251 (2007) 374.
[13] J. Rodriguez, J. Hrbek, Acc. Chem. Res. 32 (1999) 719.
[14] A. Tadd, B. Gould, J. Schwank, Catal. Today 110 (2005) 68.
[15] B. Gould, X. Chen, J. Schwank, J. Catal. 250 (2007) 209.
[16] A. Qi, S. Wang, C. Ni, D. Wu, Int. J. Hydrogen Energy 32 (2007) 981.
[17] S. Goud, W. Whittenberger, S. Chattopadhyay, M. Abraham, Int. J. Hydrogen Energy 32 (2007) 2868.
[18] P. Dinka, A. Mukasyan, J. Power Sources 167 (2007) 472.
[19] P. Cheekatamarla, A. Lane, J. Power Sources 153 (2006) 157.
[20] P. Cheekatamarla, W. Thomson, J. Power Sources 156 (2006) 520.
[21] P. Cheekatamarla, A. Lane, J. Power Sources 152 (2005) 256.
[22] K. Murata, M. Saito, M. Inaba, I. Takahara, Appl. Catal. B 70 (2007) 509.

[23] L. Wang, K. Murata, M. Inaba, Appl. Catal. B 48 (2004) 243.
[24] J. Strohm, J. Zheng, C. Song, J. Catal. 238 (2006) 309.
[25] S. Lakapati, M. Abraham, Appl. Catal. A 364 (2009) 113.
[26] Tier 2/Gasoline Sulfur Final Rule, 2000. <http://www.epa.gov/tier2/>
[27] D. Smith, US Patent 7 070 833, 2006 (to Restek Corporation).
[28] G. Barone, US Patent 6 511 760, 2003 (to Restek Corporation).
[29] D. Smith, US Patent 6 444 326, 2002 (to Restek Corporation).
[30] J. Gramshaw, A. Hussain, J. Chromatogr. 157 (1978) 267.
[31] W. Wardencki, J. Chromatogr. A 793 (1998) 1.
[32] T. Montini, A. Speghini, L. De Rogatis, B. Lorenzut, M. Bettinelli, M. Graziani, P. Fornasiero, J. Am. Chem. Soc. 131 (2009) 13155.
[33] J. Rodriguez, J. Dvorak, A. Capitano, A. Gabelnick, J. Gland, Surf. Sci. 429 (1999) 462.
[34] J. Rodriguez, Prog. Surf. Sci. 81 (2006) 141.
[35] W. Owens, N. Rodriguez, R. Baker, Catal. Today 21 (1994) 3.
[36] G. Somorjai, Surface Chemistry and Catalysis, John Wiley & Sons, New York, 2006. pp. 417.
[37] R. Horn, K. Williams, N. Degenstein, L. Schmidt, J. Catal. 242 (2006) 92.
[38] A. Qi, S. Wang, G. Fu, D. Wu, Appl. Catal., A 293 (2005) 71.
[39] S. Yoon, I. King, J. Bae, Int. J. Hydrogen Energy 33 (2008) 4780.
[40] R. Horn, K. Williams, N. Degenstein, A. Bitsch-Larsen, D. Dalle Nogare, S. Tupy, L. Schmidt, J. Catal. 249 (2007) 380.
[41] J. Nørskov, B. Clausen, H. Topsøe, Catal. Lett. 13 (1992) 1.
[42] H. Bengaard, J. Nørskov, B. Clausen, L. Nielsen, A. Molenbroek, J. Rostrup-Nielsen, J. Catal. 209 (2002) 365.
[43] E. Kümmerle, G. Heger, J. Solid State Chem. 147 (1999) 485.
[44] H. Chen, D. Zhang, G. Lu, J. Magn. Magn. Mater. 84 (1990) 208.
[45] H. Rooksby, Nature 152 (1943) 304.